

Geophysical Research Letters[®]



RESEARCH LETTER

10.1029/2021GL096666

Key Points:

- The anomalies of Leaf Area Index in 34.5% of the vegetated area in the west Pacific region were correlated to El Niño-Southern Oscillation (ENSO) index from 1982 to 2017
- The anomalies of Leaf Area Index in the west Pacific region differed significantly in Central-Pacific and Eastern-Pacific types of ENSO
- The diverse vegetation anomalies were contributed to the controls of the different types of ENSO on precipitation and temperature

Supporting Information:

Supporting Information may be found in the online version of this article.

Correspondence to:

J. Li,
lijing01@radi.ac.cn





Citation:

Wang, C., Li, J., Liu, Q., Huete, A., Li, L., Dong, Y., & Zhao, J. (2022). Eastern-Pacific and Central-Pacific types of ENSO elicit diverse responses of vegetation in the west Pacific region. *Geophysical Research Letters*, 49, e2021GL096666. <https://doi.org/10.1029/2021GL096666>

Received 29 OCT 2021

Accepted 12 JAN 2022

Eastern-Pacific and Central-Pacific Types of ENSO Elicit Diverse Responses of Vegetation in the West Pacific Region

Cong Wang^{1,2} , Jing Li^{1,3} , Qinhua Liu^{1,3}, Alfredo Huete⁴ , Longhui Li^{5,6} , Yadong Dong¹, and Jing Zhao¹

¹State Key Laboratory of Remote Sensing Science, Jointly Sponsored by Aerospace Information Research Institute, Chinese Academy of Sciences and Beijing Normal University, Beijing, China, ²Key Laboratory for Geographical Process Analysis & Simulation of Hubei Province/ School of Urban and Environmental Sciences, Central China Normal University, Wuhan, China, ³University of Chinese Academy of Sciences, Beijing, China, ⁴School of Life Sciences, University of Technology Sydney, Ultimo, NSW, Australia, ⁵Jiangsu Centre for Collaborative Innovation in Geographical Information Resource Development and Application, Nanjing Normal University, Nanjing, China, ⁶Ministry of Education Key Laboratory for Geographical Environment Evolution, Nanjing, China

Abstract The El Niño-Southern Oscillation (ENSO) is one of the main factors causing extreme climate events and, thus, has a significant influence on global climate systems. However, the long-term effects of ENSO on vegetation are not well understood due to the complexity of the ENSO phenomenon under global warming. Here, we examined the variations in the response of Leaf Area Index (LAI) to different types of ENSO from 1982 to 2017 in the west Pacific region and explored their relationship with climatic factors. Results show that about 34.5% of the vegetated area in the west Pacific region displayed LAI anomalies correlated with ENSO index from 1982 to 2017, which distributed differently across climatic types. Moreover, LAI anomalies elicited by the Central-Pacific type and by the Eastern-Pacific type of ENSO events were significantly different, which were contributed to the controls of the different types of ENSO on precipitation and temperature.

Plain Language Summary The El Niño-Southern Oscillation (ENSO), characterized by periodic fluctuations in Sea Surface Temperatures in the tropical Pacific, exerts a major influence on interannual climate variability around the world. Classical ENSO is associated with maximum anomalies in the eastern equatorial Pacific and is referred to as Eastern-Pacific (EP) type of ENSO. In recent decades, a new ENSO type, namely Central-Pacific (CP) type of ENSO, with maximum anomalies in the central equatorial Pacific, has occurred frequently. However, the relationship between ENSO types and vegetation changes is not well understood. Here, we compared satellite-based vegetation anomalies to different types of ENSO during 1982–2017 in the west Pacific region and explored their responses to climate anomalies triggered by ENSO. Results showed that the ENSO-correlated vegetated area differed across climate types in the west Pacific region. The vegetation anomalies in the CP type and the EP type showed significant differences in the west Pacific region, which were closely related to the controls of different types of ENSO on precipitation and temperature. We highlight the diverse responses of vegetation in different types of ENSO in the west Pacific region, and these findings may help our understanding of ENSO impacts on ecosystems.

1. Introduction

The El Niño-Southern Oscillation (ENSO), a recurring oscillation of coupled ocean-atmosphere dynamics in the eastern-to-central equatorial Pacific, has been recognized as one of the primary sources of interannual climate variability across the globe (McPhaden et al., 2006). In addition to neutral conditions, there are two distinct phases in sea surface temperature anomaly (SSTA): warmer (El Niño) and cooler (La Niña) ocean events. Traditionally both El Niño and La Niña were referred to as Eastern-Pacific (EP) type of ENSO, which is defined as an ENSO event when the maximum SSTA is mainly located in eastern equatorial Pacific (5°S~5°N, 150°W~90°W). During the past four decades, a CP-type of ENSO, of which the maximum SSTA is mainly located in central equatorial Pacific (5°S~5°N, 160°E~150°W), has occurred frequently (Lee & Mcphaden, 2010), which is likely in response to weakened equatorial easterlies observed over the Central Pacific (Ashok et al., 2007) or increased temperatures attributed to climate change (Yeh et al., 2009).

Many studies have indicated that El Niño/La Niña phases lead to a redistribution of precipitation and temperature patterns by affecting atmospheric circulation (Cai et al., 2011; Huang & Xie, 2015; Yang et al., 2018; Zhang

© 2022. The Authors.

This is an open access article under the terms of the [Creative Commons Attribution-NonCommercial-NoDerivs License](https://creativecommons.org/licenses/by/4.0/), which permits use and distribution in any medium, provided the original work is properly cited, the use is non-commercial and no modifications or adaptations are made.

et al., 2019). During El Niño years, warmer and drier conditions are experienced throughout many regions of the globe; Cooler, wetter conditions prevail in many regions during La Niña years (Hao et al., 2018). Furthermore, some studies have revealed that El Niño/La Niña phases have significantly affected the structure and function of vegetated ecosystems in many regions across the globe (e.g., Vicente-Serrano et al., 2006; Walther et al., 2002; Xu et al., 2011), especially near the equator (Hao et al., 2020; Ma et al., 2015; Propastin et al., 2010; Xie et al., 2019). For example, vegetation in arid and semi-arid ecosystems in Australia grew rapidly under heavy rainfall driven by the 2011 La Niña, which plays a leading role in changes of the global terrestrial carbon sink (Cai et al., 2011; Poulter et al., 2014; Zhang et al., 2017). In contrast, the millennium drought during 2001–2009 induced by El Niño was the worst in Australia since 1900s, which led to a high mortality of trees and shrubs.

However, compared with the ENSO effects on climate anomalies, the relationship between vegetation anomalies and ENSO events is less understood, as it has only been explored in recent years. Majority of previous research exploring vegetation responses to ENSO were either based on a single ENSO event or the same type of ENSO event for a specific year, due to the timing, phase, and duration of ENSO events remain largely uncertain. Long-term vegetation responses to ENSO, especially with respect to different types of ENSO (i.e., EP-type and CP-type of ENSO), have rarely been reported. Moreover, the combination of uncertainty surrounding ENSO and complexity in climatic conditions affected by ENSO through teleconnections makes it difficult to understand how vegetation will respond to ENSO and which mechanisms will drive these changes.

In this study, we examined the variations in the response of vegetation to ENSO from 1982 to 2017 in the west Pacific region between longitudes 70°E to 160°E, and from 45°N to 45°S. First, we quantified the spatial extent of the region where there have been long-term correlations between vegetation anomalies and ENSO. Second, we compared the vegetation anomalies with respect to different types (particularly EP-type and CP-type) of ENSO based on ENSO-correlated vegetated area. Finally, we investigated linkages between ENSO, climate and vegetation, for improving our understanding of vegetation variability response associated with different types of ENSO events.

2. Data Sets and Methods

2.1. Identification of ENSO Event Occurrence and Type

ENSO indices were downloaded from the National Oceanic and Atmospheric Administration Earth System Research Laboratory for the Niño 3 region (5°S~5°N, 150°W~90°W), Niño 3.4 region (5°N~5°S, 170°W~120°W), and Niño 4 region (5°S~5°N, 160°E~150°W). The average values of SSTA over the Niño 3 region and Niño 4 region from 1982 to 2017 were combined to distinguish between EP-type and CP-type ENSO using the criteria proposed by Ren and Jin (2011). The average values of SSTA over the Niño 3.4 region were used to identify El Niño/La Niña phases which are defined as a time period when five consecutive SSTA values on monthly scale were greater than 0.5°C or less than -0.5°C (Table S1 in Supporting Information S1).

2.2. Satellite Data and Pre-Processing

2.2.1. Vegetation Data Sets

We used long-term GLASS LAI data (Global Land Surface Leaf Area Index Product) as a proxy for green vegetation cover for the period from 1982 to 2017, during which 17 ENSO events were identified. The GLASS LAI datasets are contiguous both in space and time at 0.05° and 8-day resolution and have been validated to have lower uncertainty with fewer outliers for the overall biome types compared to other LAI products (Xiao et al., 2016; Xu et al., 2018). The 8-day LAI was aggregated to a monthly composite to match the temporal interval of the ENSO indices.

2.2.2. Climate Data Sets and Climate Classification Data

Temperature and precipitation observations were obtained from the ERA-Interim global reanalysis data provided by the European Centre for Medium-Range Weather Forecasts at 0.125° and 6-hourly resolution. We aggregated the original climate datasets to a monthly time scale at 0.05° resolution to match the resolution of the vegetation datasets. The Köppen-Geiger climate classification was also used in this study (Peel et al., 2007). 14 main

climatic types were selected based on specific criteria for precipitation and temperature (Table S2 in Supporting Information S1).

2.3. Correlation Assessment of Vegetation Responses to ENSO Events

The assessment of correlation between LAI variations and ENSO was conducted in three steps:

1. To avoid spurious correlations resulting from trends in the data, LAI data were linearly detrended by subtracting the long-term linear trend, obtained by using a least squares regression fit on the original time series (Ma et al., 2015; Zhu et al., 2017)
2. The standardized LAI anomaly for each month was calculated based on the z-score function (Flanagan & Adkinson, 2011; Ma et al., 2015; Xie et al., 2019)

$$Z = \frac{y_{\text{detrend}} - \mu}{\sigma} \quad (1)$$

where y_{detrend} is the monthly detrended LAI, μ and σ are the average and standard deviation of the detrended LAI for the corresponding month from 1982 to 2017. As low LAI values tend to be affected by environmental noise, to reduce uncertainty, we excluded pixels with the annual average LAI of less than 0.1.

3. The Pearson's Chi-Square test was applied to investigate the relationship between LAI anomalies and ENSO over a long time period (Lv et al., 2012). The Pearson's Chi-Square test, which evaluates the correlation between two disordered categorical variables, is calculated as follows

$$\chi^2(x, y) = \frac{(ad - bc)^2 \cdot (a + b + c + d)}{(a + b)(c + d)(a + c)(b + d)} \quad (2)$$

$$\frac{a}{a + c} > \frac{b}{b + d} \quad (3)$$

where x refers to ENSO conditions, which can be categorized as ENSO occurrences and ENSO-neutral periods based on ENSO index; y refers to vegetation variable, which can be categorized as distinct vegetation anomalies (LAI z-score ≥ 1 or ≤ -1) and non-distinct vegetation anomalies ($-1 < \text{LAI z-score} < 1$); a and b are the number of months when distinct LAI anomalies occurred during the ENSO events and ENSO-neutral periods, respectively; c and d are the number of months when non-distinct LAI anomalies occurred during the ENSO events and ENSO-neutral period, respectively. We improved the Chi-Square test by adding condition (Equation 3) to make sure that the probability of distinct LAI anomalies during the ENSO period is larger than that during the ENSO-neutral period. When χ^2 reaches the threshold χ^2_{α} ($\alpha = 0.05$ and 1 of freedom) and condition (Equation 3) is met, the LAI anomalies in this pixel are considered to be correlated with ENSO index in a long term.

2.4. Major Climatic Factors Driving Vegetation Growth

The standardized anomalies of temperature and precipitation were calculated based on steps 1 and 2 described in Section 2.3. To examine the time-lag effects of LAI anomalies to different climatic factors (refer to Wu et al., 2015), a cross correlation analysis was adopted to explore the relationship between LAI anomalies and temperature or precipitation anomalies, as follows (Xie et al., 2019):

$$cr = \frac{\sum_i^k [(x(i) - mx) * (y(i - l) - my)]}{\sqrt{\sum_i^k (x(i) - mx)^2} \sqrt{\sum_i^k (y(i - l) - my)^2}} \quad (4)$$

where cr is the cross correlation coefficient between x and y , x is the LAI anomaly time series and y is the temperature or precipitation anomaly time series; mx and my are the means of x and y , respectively; k is the total number of months; l represents the time lag of the LAI anomalies from the climate anomalies, which was considered from 0 to 3 months in the analysis following Wu et al. (2015).

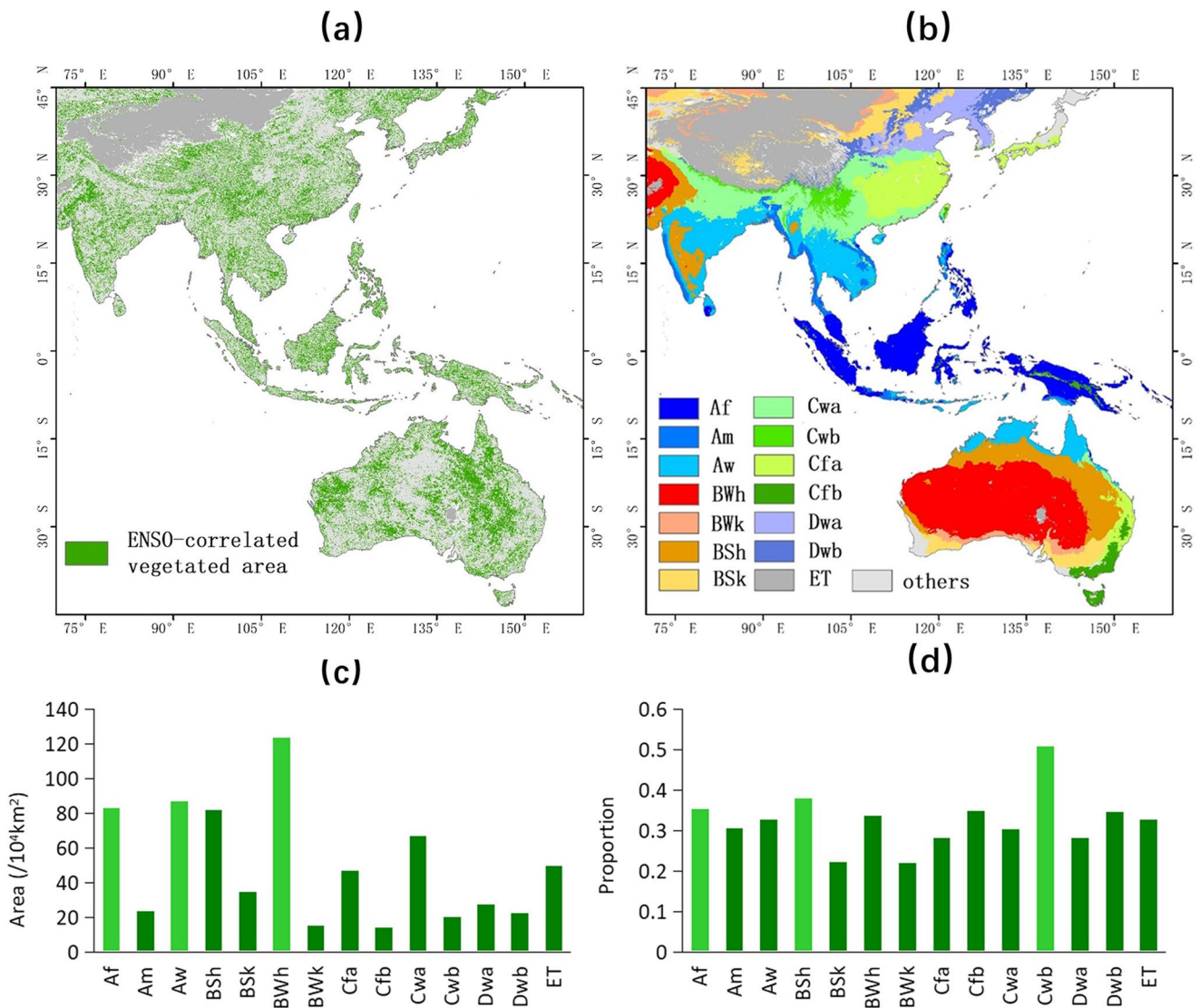


Figure 1. Spatial distribution of Leaf Area Index anomalies in (a) El Niño-Southern Oscillation periods, (b) the Köppen-Geiger climate classification, (c) the area and (d) proportion for each climate classification in the west Pacific region. The light green in (c and d) highlighted the top three climate classifications in the ranking. Af: tropical rainforest, Am: tropical monsoon, Aw: tropical savanna, BWh: arid desert hot, BWk: arid desert cold, BSh: arid steppe hot, BSk: arid steppe cold, Cwa: temperate dry winter hot summer, Cwb: temperate dry winter warm summer, Cfa: temperate without dry season hot summer, Cfb: temperate without dry season warm summer, Dwa: cold dry winter hot summer, Dwb: Cold dry winter warm summer, ET: polar tundra.

3. Results

3.1. Extent of ENSO-Correlated Vegetated Area

The vegetated area correlated to ENSO differed spatially in the west Pacific region and varied with climatic types (Figure 1). Overall, about 34.5% of the vegetated area in the west Pacific region displayed LAI anomalies correlated with ENSO index during the period from 1982 to 2017. The BWh (Arid desert hot) had the largest ENSO-correlated vegetated area (Figure 1c), where it is usually dry and the ecosystems are less complex with low structural stability and low resilience to climate change, and thus vulnerable to extreme climatic conditions. These are also supported by previous studies (Hao et al., 2020; Ma et al., 2015; Poulter et al., 2014; Propastin et al., 2010). Next was Aw (Tropical savanna), which is mainly located in northern Australia, southern Indo-China Peninsula and India. The Af (Tropical rainforest) had the third largest ENSO-correlated vegetated area (Figure 1c). Besides, more than a half of vegetated area in Cwb (Temperate dry winter warm summer) had a

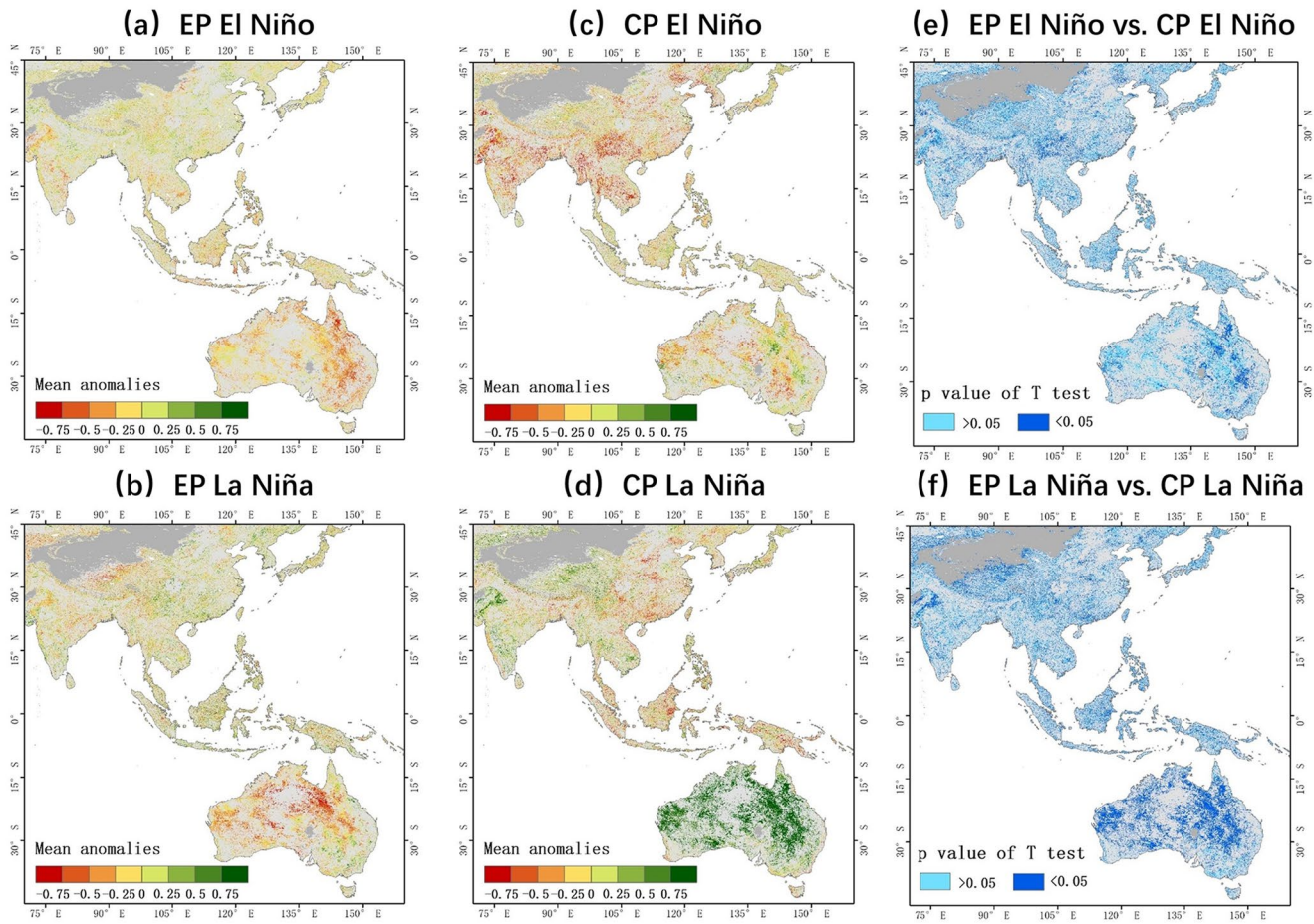


Figure 2. The mean Leaf Area Index anomalies during (a–d) different types of El Niño–Southern Oscillation in the west Pacific region. (e) Significance of the t test for the difference between vegetation anomalies in (a) EP El Niño and (c) CP El Niño, (f) significance of the t test for the difference between vegetation anomalies in (b) EP La Niña and (d) CP La Niña.

correlation with ENSO index from 1982 to 2017, which is concentrated in southwestern China; followed by BSH (Arid steppe hot) and Af (Figure 1d).

3.2. Characteristics of LAI Anomalies in Different Types of ENSO

The characteristics of LAI anomalies in different types of ENSO were analyzed based on ENSO-correlated vegetated area (Figure 2 and Figures S1 and S2 in Supporting Information S1). In general, the LAI anomalies showed diverse responses to different ENSO types in the west Pacific region (Figure 2 and Figures S1 and S2 in Supporting Information S1). In addition to warm (El Niño) and cool (La Niña) ENSO phases, we found that LAI anomalies in EP-type and CP-type of ENSO were significantly different (Figures 2e and 2f). For example, in Australia, the mean LAI anomalies in EP-type La Niña tended to have negative patterns (Figure 2b), with more than 80% of negative LAI anomalies in EP-type La Niña for most pixels (Figure S2c in Supporting Information S1); while the enhanced positive LAI anomalies in CP-type La Niña were presented, where 92.5% of pixels have an agreement with the sign of positive mean LAI anomalies (Figure 2d and Figure S2d in Supporting Information S1). Besides, the magnitude of LAI anomalies in EP-type El Niño events was higher than that in CP-type El Niño events, while LAI anomalies associated with CP-type La Niña events were stronger than in EP-type La Niña, seen especially in Australia (Figure S1 in Supporting Information S1).

3.3. Climate Drivers for LAI Anomalies in Different Types of ENSO

The anomalies in both temperature and precipitation in the west Pacific region also showed varying patterns in different ENSO types. El Niño phase tends to elevate the temperature anomaly in most areas of the west Pacific region, and this anomaly becomes even more pronounced in EP-type El Niño (Figures S3a and S3b in Supporting Information S1). La Niña phase tends to elevate the precipitation anomaly, and the anomaly is intensified in CP-type La Niña (Figures S4c and S4d in Supporting Information S1). Especially in Oceania, the temperature or precipitation anomalies showed two extremes between EP-type La Niña and CP-type La Niña (Figures S3 and S4 in Supporting Information S1), and the increased precipitation and decreased temperature lead to the increase of LAI in CP-type La Niña events (Figure 3). These precipitation and temperature anomalies tend to trigger LAI anomalies, resulting in varying spatial distribution patterns of LAI anomalies in different types of ENSO (Figures 2a–2d).

Considering that the vegetation responses to ENSO events differed spatially and varied with climatic types, we selected the BWh that had the largest ENSO-correlated vegetated area for detailed analysis (Figure 4). The LAI anomaly time series from 1982 to 2017 in BWh were negatively correlated with temperature anomaly time series ($r_{\max} = -0.42$, time lag = 2), but positively correlated with precipitation anomaly time series ($r_{\max} = 0.48$, time lag = 3), which is consistent with the findings reported in Figure 3. Figure 4b shows the distributions of LAI anomalies and their corresponding temperature anomalies (with a two-month time lag) and precipitation anomalies (with a three-months lag), which further indicates that the increased LAI anomalies are closely related with decreased temperature anomalies and increased precipitation anomalies, and vice versa. Thus, the diverse temperature and precipitation anomalies in different types of ENSO result in diverse LAI anomalies (Figure 4c). These diverse responses of LAI to CP and EP types of ENSO were also found in other climatic types in the west Pacific region (Figure S5 in Supporting Information S1).

4. Discussion

This study compared the vegetation anomalies in different types of ENSO based on ENSO-correlated vegetated area in the west Pacific region, and explored their relationship with climatic factors. We found that the LAI anomalies in CP-type and EP-type of ENSO show marked differences in the west Pacific region, and have a close relationship with different controls of CP-type and EP-type of ENSO on precipitation and temperature. These findings highlight the diverse response of vegetation to EP or CP type of ENSO, improving our understanding of ENSO impacts on ecosystems for better coping with climate change (Collins et al., 2010; Yuan et al., 2020).

We mapped ENSO-correlated vegetated area for the west Pacific region from 1982 to 2017 based on the improved Chi-Square test. The ENSO-correlated vegetated area was dispersed especially in Asia, possible reasons include: (a) The vegetated landscape has a complex and mosaic distribution pattern developed by fragmentation and intersection of various vegetation patches (Su et al., 2020), which results in a scattered distribution of ENSO-correlated area; (b) The spatial distributions of climate types, topography, and human activities vary, which also leads to heterogeneous spatial patterns in vegetation responses to ENSO; (c) There has been extensive land cover change from 1982 to 2017, especially in agriculture and urban areas (Gong et al., 2019; Liu et al., 2014), which may have weakened the vegetation correlation with ENSO events in these areas. Besides, different data sources and data processing methods (i.e., detrending, anomaly calculation) would also affect the identification of ENSO-correlated area. However, the LAI anomalies derived from MODIS and AVHRR sensors still present similar opposite responses of vegetation to EP-type and CP-type La Niña events in Australia (Figure S4 in Supporting Information S1), and the overlapping region still covers about 62.2% of area when using different detrending methods (Figure S5 in Supporting Information S1). This indicates that different LAI products and detrending methods will have an influence on the identification of ENSO-correlated vegetated area, but the area closely correlated with ENSO events tends to remain consistent since the vegetation anomalies in ENSO-correlated area are higher than the LAI errors introduced by the product algorithms and detrending methods.

Preceding studies have demonstrated that the CP and EP types of ENSO are fundamentally different in terms of their evolution, occurrence mechanisms, and climate impacts (Kao & Yu, 2009; Kim & Yu, 2012; Yu et al., 2011; Yu & Kim, 2010). The active convection area for CP ENSO events develops west of the convection area associated with EP ENSO events, forming two anomalous Walker circulation circles over the equatorial Pacific. This circulation change resulted in an influence on climate anomalies opposite to that of EP ENSO events (Kao &

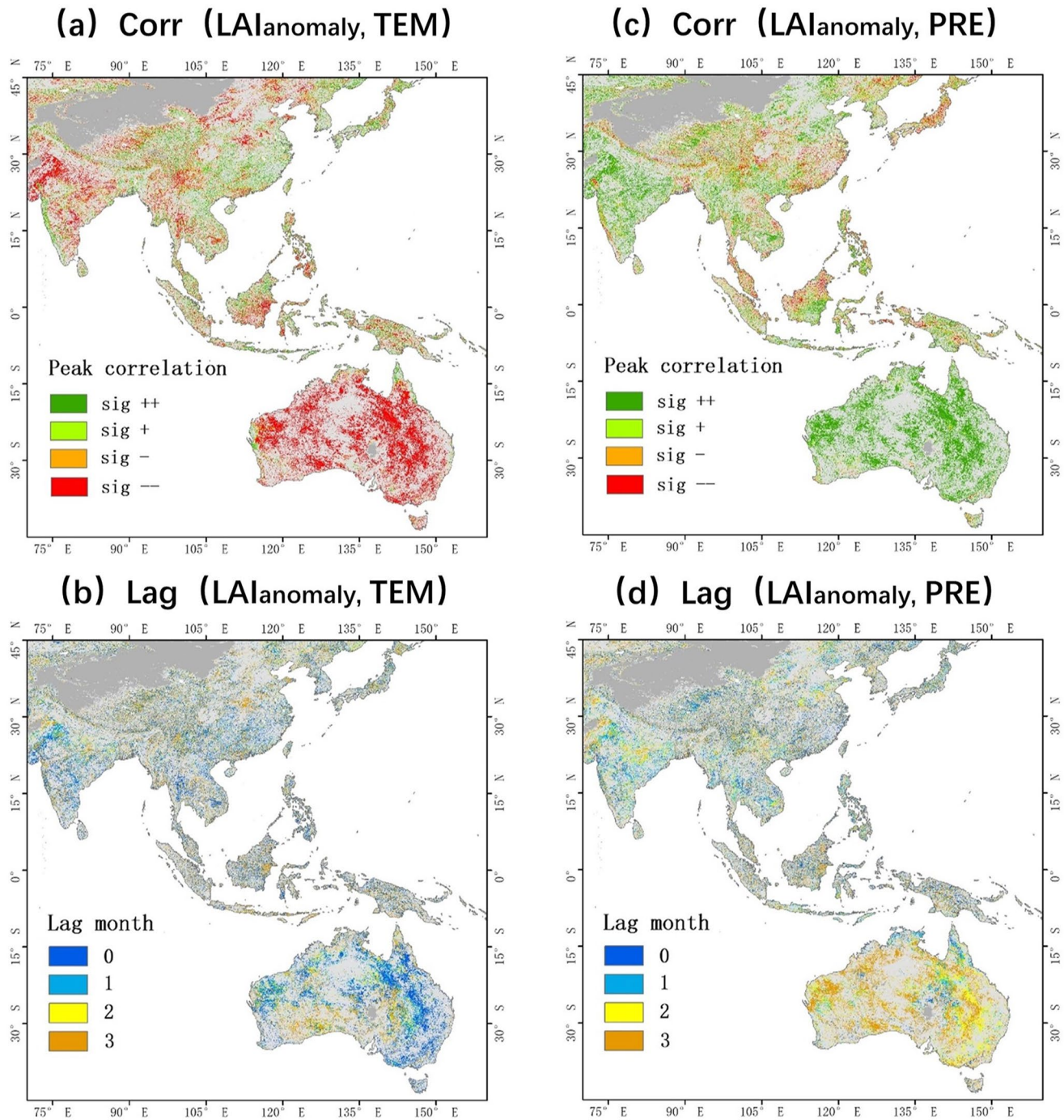


Figure 3. The temperature and precipitation effects on Leaf Area Index anomalies in terms of the peak correlation (a and c) and the corresponding lag time (b and d). The legends Sig ++ and Sig -- in (a) and (c) indicate significant positive and negative correlations ($p < 0.05$), respectively, while Sig + and Sig - represent nonsignificant correlations ($p > 0.05$).

Yu, 2009; Kim & Yu, 2012; Yu et al., 2011). For example, it has been shown that southern China experiences increased rainfall in the following spring and summer when EP El Niño events occur but reduced rainfall in those same seasons during CP El Niño events (Feng & Li, 2011). These supported our findings of diverse response of vegetation to EP and CP types of ENSO. Furthermore, the newly emerging CP type of ENSO significantly enhances the atmospheric oscillation in last four decades. The shift between EP-type and CP-type of ENSO is to some extent resulted in the increasing frequency and severity of weather extremes (e.g., droughts, floods and

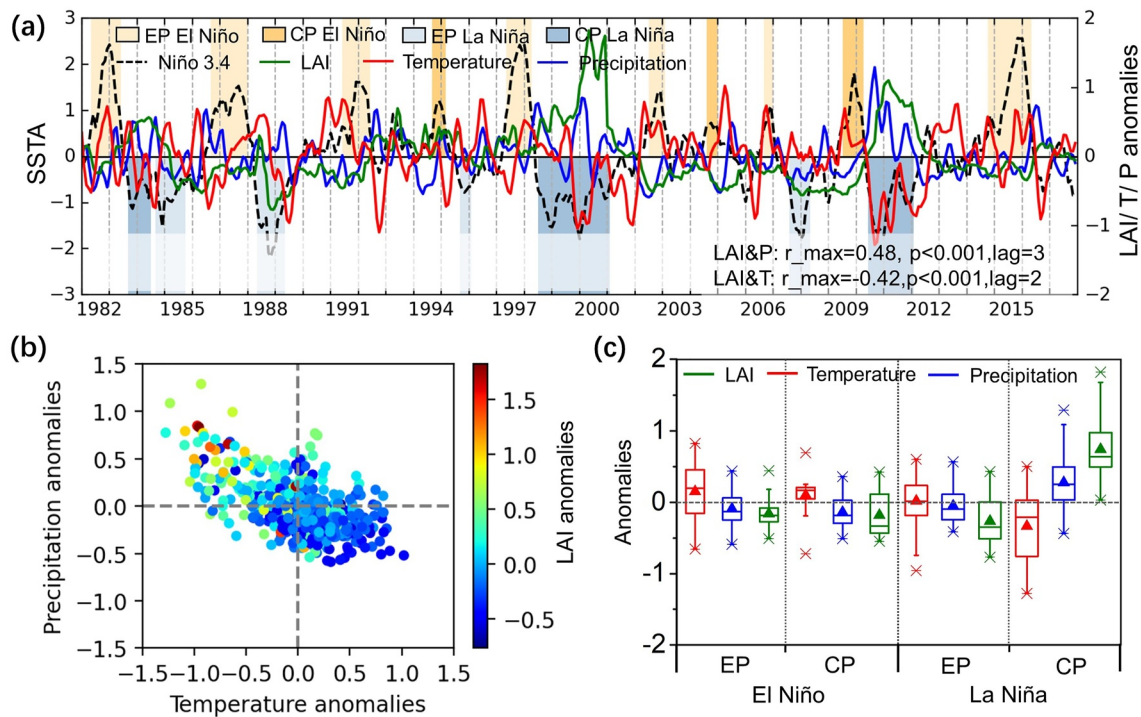


Figure 4. Relationship between Leaf Area Index (LAI) anomalies and precipitation or temperature anomalies in BWh during different types of El Niño-Southern Oscillation. Time series of LAI, precipitation and temperature anomalies (a) and their distributions (b and c). The r_{\max} and lag in (a) is the maximum Person's correlation coefficient between LAI anomaly and temperature or precipitation anomaly time series and the corresponding time lag.

heatwaves) in many global locations, which enlarges the interannual fluctuation of vegetation growth, and challenges the sustainable growth of ecosystems in some climate zones.

It should be noted that, although vegetation anomalies during ENSO-neutral periods were excluded from our analyses, other periodic atmospheric oscillations (e.g., the Indian Ocean dipole, Arctic Oscillation) and human activities also affect vegetation anomalies during the ENSO period (Cai et al., 2011; Xie et al., 2019). Data processing is computation-intensive, we therefore have chosen the LAI as a proxy for vegetation for the analysis in this study. In the future, additional vegetation variables from multi-source/sensors, such as normalized difference vegetation index, solar-induced chlorophyll fluorescence, gross primary productivity, could be used to reduce the uncertainty in vegetation growth anomalies. Considering the universal influence of ENSO, further research should examine the variations in responses of vegetation to EP and CP types of ENSO in other regions at the global scale. Moreover, the underlying mechanisms of different types of ENSO need to be further explored, to provide additional evidence for the long-term influence of ENSO on vegetation and ecosystems across the globe.

5. Conclusions

This study examined the variations in the response of vegetation to different types of ENSO in the west Pacific region from 1982 to 2017 and investigated linkages between ENSO, climate and vegetation. We found that, in addition to warm (El Niño) and cool (La Niña) ENSO phases, the responses of vegetation to CP-type and EP-type of ENSO demonstrate significant differences in the west Pacific region, which are closely related with different controls of CP-type and EP-type of ENSO on precipitation and temperature. Our findings highlight the diverse responses of vegetation in different types of ENSO in the west Pacific region, which will enhance our understanding of the impact of ENSO on ecosystems thus warrant further studies at the global scales.

Data Availability Statement

ENSO indices data sets are available from https://www.esrl.noaa.gov/psd/gcos_wgsp/Timeseries/. GLASS LAI is available at <http://glass-product.bnu.edu.cn/introduction/LAI.html> (only available in Chinese). The temperature/precipitation datasets are from <https://apps.ecmwf.int/datasets/data/interim-full-daily/levtype=sfc/>. Köppen-Geiger climate classification map is downloaded from (www.gloh2o.org/koppen).

Acknowledgments

This work was supported by National Key Research and Development Program (2019YFE0126700), National Natural Science Foundation of China (42101391), Global Ecosystem and Environment Observation Analysis Research Cooperation (GEOARC) by National Remote Sensing Center of China, and Fundamental Research Funds for the Central Universities (CCNU21XJ028).

References

- Ashok, K., Behera, S., Rao, S. A., Weng, H., & Yamagata, T. (2007). El Niño Modoki and its teleconnection. *Journal of Geophysical Research*, *112*, C11007. <https://doi.org/10.1029/2006jc003798>
- Cai, W., Rensch, P., Cowan, T., & Hendon, H. (2011). Teleconnection pathways of ENSO and the IOD and the mechanisms for impacts on Australian rainfall. *Journal of Climate*, *24*, 3910–3923. <https://doi.org/10.1175/2011jcli4129.1>
- Collins, M., An, S. I., Cai, W., & Ganachaud, A. (2010). The impact of global warming on the tropical Pacific Ocean and El Niño. *Nature Geoscience*, *3*, 391–397. <https://doi.org/10.1038/ngeo868>
- Feng, J., & Li, J. (2011). Influence of El Niño Modoki on spring rainfall over south China. *Journal of Geophysical Research*, *116*, D13102. <https://doi.org/10.1029/2010jd015160>
- Flanagan, L. B., & Adkinson, A. C. (2011). Interacting controls on productivity in a northern Great Plains grassland and implications for response to ENSO events. *Global Change Biology*, *17*(11), 3293–3311. <https://doi.org/10.1111/j.1365-2486.2011.02461.x>
- Gong, P., Li, X., & Zhang, W. (2019). 40-year (1978–2017) human settlement changes in China reflected by impervious surfaces from satellite remote sensing. *Science Bulletin*, *64*, 756–763. <https://doi.org/10.1016/j.scib.2019.04.024>
- Hao, Y., Hao, Z., Feng, S., Zhang, X., & Hao, F. (2020). Response of vegetation to El Niño–Southern Oscillation (ENSO) via compound dry and hot events in southern Africa. *Global and Planetary Change*, *195*, 103358. <https://doi.org/10.1016/j.gloplacha.2020.103358>
- Hao, Z., Hao, F., Singh, V. P., & Zhang, X. (2018). Quantifying the relationship between compound dry and hot events and El Niño–Southern Oscillation (ENSO) at the global scale. *Journal of Hydrology*, *567*, 332–338. <https://doi.org/10.1016/j.jhydrol.2018.10.022>
- Huang, P., & Xie, S. P. (2015). Mechanisms of change in ENSO-induced tropical pacific rainfall variability in a warming climate. *Nature Geoscience*, *8*, 922–926. <https://doi.org/10.1038/ngeo2571>
- Kao, H., & Yu, J. (2009). Contrasting Eastern-Pacific and Central-Pacific types of ENSO. *Journal of Climate*, *22*, 615–632. <https://doi.org/10.1175/2008jcli2309.1>
- Kim, S. T., & Yu, J. Y. (2012). The two types of ENSO in CMIP5 models. *Geophysical Research Letters*, *39*, 221–228. <https://doi.org/10.1029/2012gl0152006>
- Lee, T., & Mcphaden, M. J. (2010). Increasing intensity of El Niño in the central-equatorial pacific. *Geophysical Research Letters*, *37*(14), L14603. <https://doi.org/10.1029/2010gl044007>
- Liu, J., Kuang, W., Zhang, Z., & Xu, X. (2014). Spatiotemporal characteristics, patterns and causes of land use changes in China since the late 1980s. *Journal of Geographical Sciences*, *24*, 195–210. <https://doi.org/10.1007/s11442-014-1082-6>
- Lv, A., Zhu, W., & Jia, S. (2012). Assessment of the sensitivity of vegetation to El-Niño/Southern Oscillation events over China. *Advances in Space Research*, *50*, 1362–1373.
- Ma, X., Huete, A., Moran, S., & Ponce-Campos, G. E. (2015). Abrupt shifts in phenology and vegetation productivity under climate extremes. *Journal of Geophysical Research: Biogeosciences*, *120*, 2036–2052. <https://doi.org/10.1002/2015jg003144>
- Mcphaden, M. J., Zebiak, S. E., & Glantz, M. H. (2006). ENSO as an integrating concept in earth science. *Science*, *314*, 1740. <https://doi.org/10.1126/science.1132588>
- Peel, M. C., Finlayson, B. L., & McMahon, T. A. (2007). Updated world map of the Köppen-Geiger climate classification. *Hydrology and Earth System Sciences*, *4*(2).
- Poulter, B., Frank, D., Ciais, P., Myneni, R. B., Andela, N., Bi, J., et al. (2014). Contribution of semi-arid ecosystems to interannual variability of the global carbon cycle. *Nature*, *509*, 600. <https://doi.org/10.1038/nature13376>
- Propastin, P., Fotso, L., & Kappas, M. (2010). Assessment of vegetation vulnerability to ENSO warm events over Africa. *International Journal of Applied Earth Observations & Geoinformation*, *12*, S83–S89. <https://doi.org/10.1016/j.jag.2009.10.007>
- Ren, H., & Jin, F. (2011). Niño indices for two types of ENSO. *Geophysical Research Letters*, *38*(4), L04704. <https://doi.org/10.1029/2010gl046031>
- Su, Y., Guo, Q., Hu, T., Guan, H., Jin, S., An, S., et al. (2020). An updated vegetation map of China (1:1000000). *Science Bulletin*, *65*, 1125–1136. <https://doi.org/10.1016/j.scib.2020.04.004>
- Vicente-Serrano, S. M., Delbart, N., & Toan, L. T. (2006). El Niño–Southern Oscillation influences on the interannual variability of leaf appearance dates in central Siberia. *Geophysical Research Letters*, *33*. <https://doi.org/10.1029/2005gl025000>
- Walther, G. R., Post, E., Convey, P., Menzel, A., Parmesan, C., Beebee, T. J. C., et al. (2002). Ecological responses to recent climate change. *Nature*, *416*, 389–395. <https://doi.org/10.1038/416389a>
- Wu, D., Zhao, X., Liang, S., Zhou, T., Huang, K., Tuang, B., & Zhao, W. (2015). Time-lag effects of global vegetation responses to climate change. *Global Change Biology*, *21*, 3520–3531. <https://doi.org/10.1111/gcb.12945>
- Xiao, Z., Liang, S., Wang, J., & Xiang, Y. (2016). Long-time-series global land surface satellite leaf area index product derived from MODIS and AVHRR surface reflectance. *IEEE Transactions on Geoscience and Remote Sensing*, *54*(9), 5301–5318. <https://doi.org/10.1109/tgrs.2016.2560522>
- Xie, Z., Huete, A., Cleverly, J., Phinn, S., McDonald-Madden, E., Cao, Y., & Qin, F. (2019). Multi-climate mode interactions drive hydrological and vegetation responses to hydroclimatic extremes in Australia. *Remote sensing of Environment*, *231*, 111270. <https://doi.org/10.1016/j.rse.2019.111270>
- Xu, B., Li, J., Park, T., & Liu, Q. (2018). An integrated method for validating long-term leaf area index products using global networks of site-based measurements. *Remote Sensing of Environment*, *209*, 134–151. <https://doi.org/10.1016/j.rse.2018.02.049>
- Xu, L., Samanta, A., Costa, M. H., Ganguly, S., Nemani, R. R., & Myneni, R. B. (2011). Widespread decline in greenness of Amazonian vegetation due to the 2010 drought. *Geophysical Research Letters*, *38*, L07402. <https://doi.org/10.1029/2011gl046824>
- Yang, S., Li, Z., Yu, J. Y., Hu, X., Dong, W., & He, S. (2018). El Niño-southern oscillation and its impact in the changing climate. *National Science Review*, *5*, 840–857. <https://doi.org/10.1093/nsr/nwy046>
- Yeh, S. W., Kug, J. S., Dewitte, B., & Kwon, M. H. (2009). El Niño in a changing climate. *Nature*, *462*(7273), 674. <https://doi.org/10.1038/nature08546>

- Yu, J., Kao, H., Tong, L., & Kim, S. T. (2011). Subsurface ocean temperature indices for Central-Pacific and eastern-pacific types of El Niño and La Niña Events. *Theoretical and Applied Climatology*, 103(3–4), 337–344. <https://doi.org/10.1007/s00704-010-0307-6>
- Yu, J., & Kim, S. (2010). *Transitions between Central-Pacific and eastern-pacific types of ENSO* (pp. 1277). AGU Fall Meeting Abstracts.
- Yuan, M., Zhu, Q., Zhang, J., Liu, J., Chen, H., Peng, C., et al. (2020). Global response of terrestrial gross primary productivity to climate extremes. *The Science of the Total Environment*, 750, 142337.
- Zhang, A., Jia, G., Epstein, H., & Jiangjiang, X. (2017). ENSO elicits opposing responses of semi-arid vegetation between Hemispheres. *Scientific Reports*, 7, 42281. <https://doi.org/10.1038/srep42281>
- Zhang, Y., Dannenberg, M. P., Hwang, T., & Song, C. (2019). El Niño–Southern Oscillation-induced variability of terrestrial gross primary production during the satellite era. *Journal of Geophysical Research: Biogeosciences*, 124(8), 2419–2431. <https://doi.org/10.1029/2019jg005117>
- Zhu, Z., Piao, S., Xu, Y., Bastos, A., Ciais, P., & Peng, S. (2017). The effects of teleconnections on carbon fluxes of global terrestrial ecosystems. *Geophysical Research Letters*, 44(7), 3209–3218. <https://doi.org/10.1002/2016gl071743>